Possible Causes of the Interdecadal Transition of the Somali Jet Around the Late 1990s

XIAO Ziniu[1,2] (肖子牛), SHI Wenjing[1,2,4*] (石文静), and YANG Ping[3] (杨 萍)

1 *Department of Atmospheric Science, Nanjing University of Information Science & Technology, Nanjing* 210044, *China*

2 *State Key Laboratory of Numerical Modeling for Atmospheric Sciences and Geophysical Fluid Dynamics, Institute of Atmospheric Physics, Chinese Academy of Sciences, Beijing* 100029, *China*

3 *China Meteorological Administration Training Center, Beijing* 100081, *China*

4 *Cooperative Institute for Meteorological Satellite Studies, University of Wisconsin-Madison, Madison, WI* 53706, *USA*

(Received October 15, 2014; in final form December 11, 2014)

ABSTRACT

This observational study demonstrates that the Somali jet (SMJ) experienced a notable interdecadal transition in not only its lower-level parts (< 850 hPa) but also its higher-level parts (850–600 hPa) in the late 1990s. The results also show that the jet at higher level is more significantly related to East Asian monsoon rainfall than that at lower level. Thus, a new whole-layer SMJ (WSMJ) index which includes variations of the higher-level jet is defined based on the average meridional wind speed at five levels (1000–600 hPa). The interdecadal transition of the SMJ can be mainly attributed to the meridional thermal contrast anomalies near the equator which are associated with the three-pole pattern of the southern Indian Ocean.

Key words: interdecadal transition, Somali jet, index, Asian summer monsoon, southern Indian Ocean, sea surface temperature

Citation: Xiao Ziniu, Shi Wenjing, and Yang Ping, 2015: Possible causes of the interdecadal transition of the Somali jet around the late 1990s. *J. Meteor. Res.*, **29**(2), 214–227, doi: 10.1007/s13351-015-4103-1.

1. Introduction

The low-level monsoon circulation over the western Indian Ocean is characterized by southeasterly trade winds in the Southern Hemisphere, a strong and narrow cross-equatorial flow (CEF) off the coast of Somalia, and southwesterly winds over the Arabian Sea. The low-level cross-equatorial flow, often known as the Somali jet (SMJ), is an important channel for mass, momentum, and heat exchange between the Northern and Southern hemispheres, and acts as a "bridge" for weather and climate between the hemispheres. This low-level strong current is most pronounced at about 700 hPa, has its core at approximately 925 hPa (Qian et al., 1987; Chakraborty et al., 2009; Pu and Cook, 2010), and was discovered early in the mid 1960s (Bunker, 1965; Joseph and Raman, 1966). Findlater (1969a, b) first showed that the SMJ located between 38° and 55°E originates from trade wind easterlies over the southern Indian Ocean, crosses the equator along a narrow longitudinal belt over the Somali coast, and turns towards India as a westerly current close to the Arabian Sea. SMJ changes on multiple timescales, not just seasonally, but also interannually and interdecadally (Boos and Emanuel, 2009; Pu and Cook, 2010). Although the SMJ is the strongest CEF, the magnitude of its interannual variation is smaller than that of other CEFs in the Eastern Hemisphere (Lei and Yang, 2008; Tang et al., 2009). The interdecadal variation of the SMJ is greater than its year-to-year

Supported by the National Natural Science Foundation of China (41175051 and 41375069), National Basic Research and Development (973) Program of China (2012CB957804), Postgraduate Science and Technology Innovation Project of Jiangsu Province (CXZZ13_0517), and the China Scholarship Council (CSC).

*Corresponding author: shiwenjing_005@163.com.

variations (Zhu, 2012). Shi et al. (2007) found that the strength of the SMJ increases, on average, by 0.25 m s^{-1} per decade.

As part of the monsoon system (Ding, 2005), the intensity of the SMJ was found to be positively related to the amount of rainfall in most regions of India, especially in the monsoon regions on both interannual and interdecadal timescales (Findlater, 1977; Cadet and Desbois, 1981; Halpern and Woiceshyn, 2001; Cong et al., 2007). A stronger SMJ was related to southwesterly wind anomalies over the Arabian Sea, which can bring more water vapor to the Indian summer monsoon region (Chakraborty et al., 2009) and thus more rainfall over most regions of India. Krishnamurti et al. (1976) also considered that cross-equatorial winds are stronger during a strong Indian monsoon than during a weak one. Traditionally, the energy of the SMJ will be dispersed northeastward, bringing large amounts of water vapor to the East Asian summer monsoon regions (Shi et al., 2001; Wang and Xue, 2003; Wang and Yang, 2008; Shi and Xiao, 2013; Dai and Xiao, 2014), but no strong connection has been found between the SMJ and East Asian summer rainfall on interannual timescales (Lei and Yang, 2008; Zhu, 2012). However, on the interdecadal timescale, the link between SMJ intensity and East Asian summer rainfall shows a positive correlation over north of the Yangtze River, but a negative correlation over south of the Yangtze River (Zhu, 2012). In addition, the variability of the SMJ is also associated with the location of the western Pacific subtropical high, ENSO, and the Pacific decadal oscillation (PDO; Chen et al., 2005; Wang and Yang, 2008).

Several factors have been linked to SMJ formation, including the East African Mountains, the beta effect, land-sea contrast, baroclinicity in the boundary layer, and diabatic heating (Krishnamurti et al., 1976; Hart, 1977; Bannon, 1979a, b; Krishnamurti and Wong, 1979; Bannon, 1982; Li et al., 2006; Xu et al., 2010). Using a primitive equation model with specified zonal flow, orography, and diabatic heating, Rodwell and Hoskins (1995) determined that the land-sea contrast caused by orography plays an important role in SMJ strength variability. Chakraborty et al. (2009) suggested that the SMJ can occur even in the absence of African orography. Therefore, the cause and effect correlation between the thermal state of the oceans and SMJ variation remain a matter of debate.

Recently, the interdecadal shift of climate occurring in the late 1990s has become a focus of study. For example, Wu et al. (2012) found that September Arctic sea ice extent (SIE) showed a pronounced negative trend over the past two decades, and summer (July–September) Arctic surface wind pattern experienced an interdecadal shift in the late 1990s. Additionally, sea surface temperatures (SSTs) in North Atlantic and summer atmospheric circulation over Eurasia also exhibited an interdecadal shift in the late 1990s (Honda et al., 2009; Wu et al., 2013). Actually, some studies found that the vertical structure of the SMJ also showed an interdecadal variation around 1995 (Qiu and Sun, 2013; Xie et al., 2013; Qiu et al., 2014). Zhu (2012) suggested that the Somali CEFs above 850 hPa showed a strong upward trend in the late 1990s, based on analysis of data for the period 1950–2010.

Despite many previous studies, open questions remain and further research is required. To characterize the strength of the SMJ, a jet index has previously been defined as the area-average of the JJA (June–July–August) 925- or 850-hPa meridional wind speed around Somalia (Findlater, 1969a; Li and Lou, 1987; Wang and Xue, 2003; Lin et al., 2008; Wang and Yang, 2008). However, little attention has been paid to the higher-level component of the SMJ (i.e., the southerly jet above 850 hPa). Therefore, in this study, we focus on the vertical structure of the SMJ, especially the variation of the higher-level jet. To characterize the strength of the SMJ, we established a new jet index based on the whole-layer meridional wind speed, and investigated its influence on the Asian summer monsoon. Finally, we also evaluated possible reasons for the interdecadal transition of the vertical structure of the SMJ around 1995. The data used in this study were mainly from the NCEP/NCAR reanalysis dataset (Kalnay et al., 1996). As satellite data were incorporated into the reanalysis after the late 1970s (Sterl, 2004), which increases the reliability of the reanalysis, we focus here on the period 1979–2013.

The remainder of the paper is organized as follows. Section 2 outlines the data used in this study.

Section 3 describes the temporal features and vertical structure of the SMJ during the period 1979–2013, as well as its connection with the Asian summer monsoon. Possible reasons for the interdecadal transition of the SMJ vertical structure in the late 1990s are presented in Section 4, and Section 5 presents the conclusions.

2. Data and approach

The primary atmospheric parameters considered in this study are wind speed (m s^{-1}) and air temperature (℃) at 17 standard pressure levels, as well as vertical wind speed (Pa s^{-1}) at 12 standard pressure levels, obtained from the NCEP/NCAR reanalysis dataset (Kalnay et al., 1996) on a monthly timescale and with a spatial resolution of 2.5° × 2.5°. Because of substantial differences between the NCEP/NCAR reanalysis and the ECMWF reanalysis products, particularly around the SMJ region (Annamalai et al., 1999), monthly wind data from the higher-resolution (1.5° × 1.5°) ECMWF Interim Re-Analysis (ERA-Interim; Simmons et al., 2007) were also used for comparison.

The precipitation datasets include: (1) monthly mean precipitation reconstruction data (PREC; Chen et al., 2002; 2.5° × 2.5°; mm day^{-1}) provided by the National Oceanic and Atmospheric Administration (NOAA)/Climate Prediction Center (CPC), and (2) the monthly mean Global Precipitation Climatology Center monitoring product (GPCC; Rudolf et al., 1994; 1.0° × 1.0°; mm) data. We obtained monthly mean SST data (℃) from the NOAA extended reconstructed SST 2° × 2° dataset (Smith and Reynolds, 2004). All datasets cover the period 1979–2013. Summer is defined as the average from June to August. Statistical treatment of the data was based on correlation analysis, composite analysis, and sliding correlation analysis verified by Student's *t*-test.

3. Variations in summer SMJ intensity and its influence on the Asian summer monsoon

3.1 Temporal evolution and vertical structure

Located over the equator at 40°–55°E, the SMJ is the strongest of the Eastern Hemisphere CEFs and is most prominent during JJA. To reflect the temporal evolution and vertical structure of SMJ intensity, the areal mean (40°–55°E at the equator) meridional wind speed and anomalies in summer at different levels were calculated. This averaging region was selected to capture the maximum southerly wind speed over the eastern coast of Kenya. Figure 1a shows that the SMJ has maximum wind speeds (> 10 m s^{-1}) at about 925 hPa, and extends from surface to 600 hPa (Gao and Xue, 2006; Boos and Emanuel, 2009; Chakraborty et al., 2009). From the late 1990s, the vertical spread of the stronger SMJ (> 2 m s^{-1}) significantly increased to above 600 hPa. As shown in Fig. 1a, the higher-level (850, 700, and 600 hPa) jet intensities were persistently lower than normal before the late 1990s, but above normal after that. By contrast, variations in the lower-level (1000 and 925 hPa) jet intensity followed an opposite pattern. Although the SMJ was much stronger at 925 hPa (the maximum meridional wind speed was over 10 m s^{-1}) than at 700 hPa (the maximum meridional wind speed was about 3 m s^{-1}), the standard deviation (SD) of the latter was much higher (925 hPa, SD = 0.53, 700 hPa, SD = 1.53; Fig. 1b). The amplitude of the variation in the higher-level jet is much greater than that in the lower-level jet, as pointed out by Qiu and Sun (2013).

To better characterize the overall strength of the SMJ at five levels (from 1000 to 600 hPa), a whole-layer SMJ (WSMJ) index was defined as the area and vertical average of the JJA meridional wind speed between 1000 and 600 hPa over the area 40°–55°E at the equator. The time series of the WSMJ index (solid curve) is shown in Fig. 1c. Compared with the WSMJ index, the time series (dashed curve) of the jet index at 925 hPa (as traditionally defined in previous studies; e.g., Tang et al., 2009) and the difference (bar) between the two indices, are also displayed in Fig. 1c. The WSMJ index and the jet index at 925 hPa both exhibit apparent interannual and interdecadal variations. However, there are great differences between them (shown by the bars), which are caused by the different methods used to calculate the two indices. The WSMJ index is below normal before the late 1990s

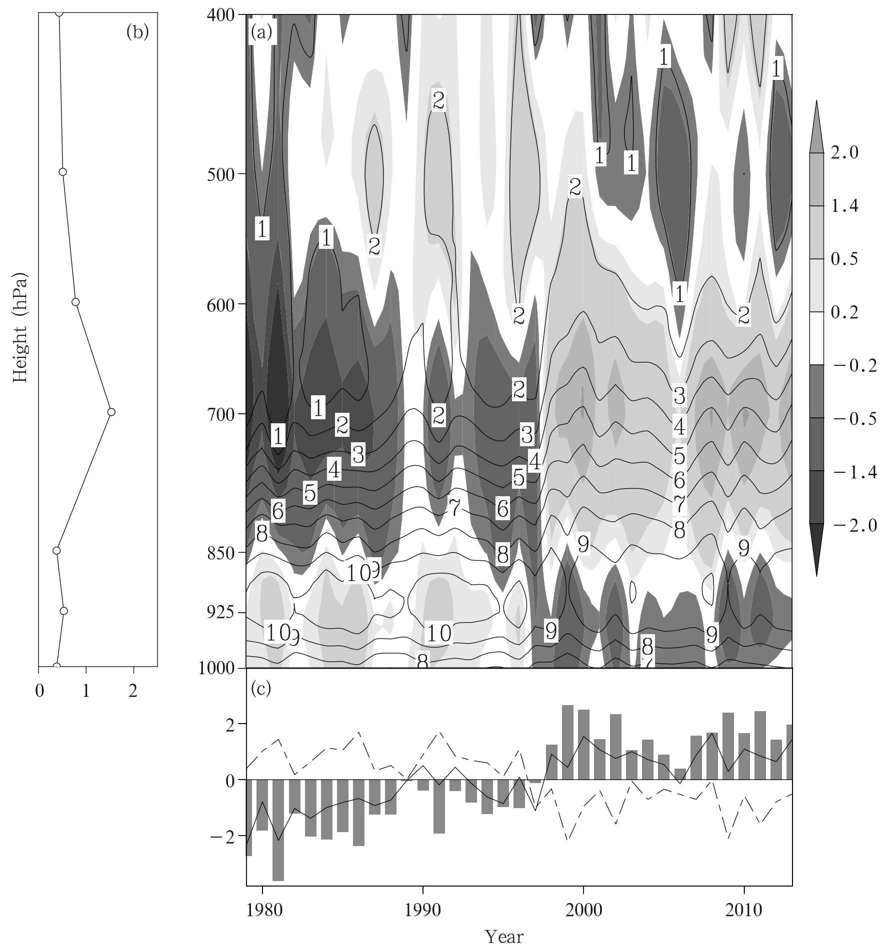

Fig. 1. (a) Areal mean meridional wind speed (contour; interval 1 m s^{-1}) and anomalies (shaded) at different levels in summer over the SMJ region (40°–55°E at the equator) between 1979 and 2013. (b) Vertical profile of the standard deviation of the jet at different levels. (c) Normalized time series of the summer WSMJ index (solid curve), the jet index at 925 hPa (dashed curve), and their difference (grey bar; WSMJ index minus jet index at 925 hPa) for 1979–2013.

and above normal after that, while the jet index at 925 hPa just reverses. There is an interdecadal transition point around the late 1990s in the vertical structure of the SMJ.

This interdecadal transition can be further confirmed by using the dominant mode (that explains about 55.1% of the total variance) of the time-altitude cross-section of the SMJ intensity anomalies (Fig. 1a; shaded) through an empirical orthogonal function (EOF) analysis based on the NCEP/NCAR reanalysis data (Fig. 2). This analysis shows that the higher-level and lower-level jet changes are out of phase. As for the corresponding time coefficient (Fig. 2b), there is evident interdecadal variability. The time series is negative from the 1980s to the late 1990s, but positive from the late 1990s to the present. In combination with Fig. 2a, it is suggested that the lower-level jet intensities are decreasing while higher-level jet intensities are increasing.

To isolate the decadal signal, the 9-yr running means of the jet intensity anomalies at different levels from the NCEP/NCAR reanalysis and ERA-Interim datasets are displayed in Figs. 3a and 3b, respectively. Decadal variations of the jet intensities at different levels are similar to those shown by Qiu and Sun (2013) and Qiu et al. (2014), who examined the vertical structure of the SMJ in summer. By comparison, the magnitudes of the NCEP/NCAR jet intensities are much larger than those of the ERA-Interim jet intensities at any level. At the higher levels (850–600 hPa), their

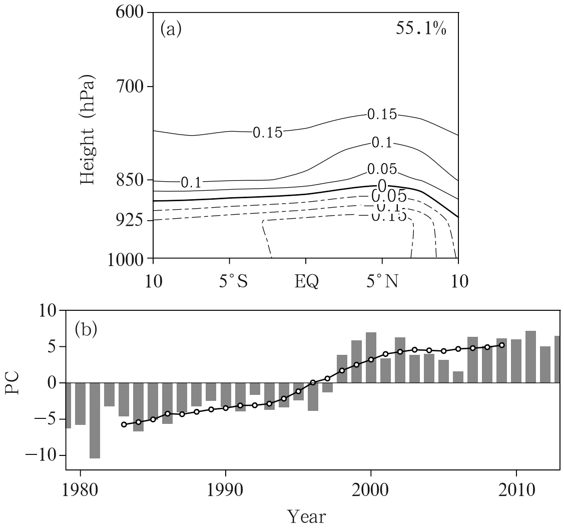

Fig. 2. (a) First EOF of the JJA meridional wind anomalies averaged over 40°–55°E and (b) PC1 of the EOF decomposition (bar) and its 9-yr running mean (curve).

spatial distributions are similar. While there are obvious differences at lower levels (< 850 hPa), common features are also visible. As stated by Pu (2012), many factors may contribute to the differences among the reanalysis datasets; for example, different sources of observations, physical parameterizations used in models and assimilation methods.

To investigate the linkage between the lower- and higher-level jets, correlations among all combinations of jet indices at 1000, 925, 850, 700, and 600 hPa were calculated (Table 1). The correlation coefficient between jet indices at 1000 and 925 hPa is 0.892, significant at the 99% confidence level. Furthermore, correlation coefficients among jet indices at 850, 700, and 600 hPa all exceed the 99% confidence level, except for that between 850 and 600 hPa, which exceeds the 95% confidence level. Therefore, in this study, the lower-level jet is between 1000 and 925 hPa, while the higher-level jet is between 700 and 600 hPa. The transition layer is 850 hPa.

Table 1. Correlation coefficients among jet indices at 1000, 925, 850, 700, and 600 hPa

	925 hPa	850 hPa	700 hPa	600 hPa
1000 hPa	**0.892**	–0.051	**–0.720**	**–0.567**
925 hPa		–0.010	**–0.758**	**–0.587**
850 hPa			**0.552**	*0.344*
700 hPa				**0.841**

Note: Values significant at the 95% and 99% confidence levels are in italics and bold, respectively.

Equally notable is that the correlation coefficient between the lower- and higher-level jets is negative, implying that their variations are out of phase, which is consistent with the above analysis. The jet at the transition layer is insignificantly related to the lower-level jet.

3.2 Correlation with East Asian summer monsoon rainfall

The analysis above reveals that the jet intensity at higher levels also shows significant year-to-year changes. To emphasize the significance of the higher-

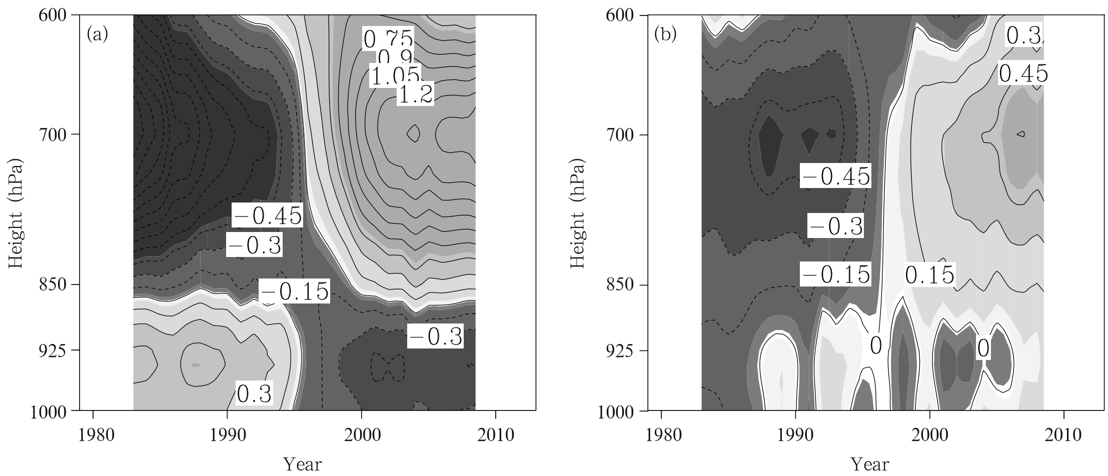

Fig. 3. Altitude-time cross-section of the 9-yr running mean summer SMJ intensity anomalies from (a) NCEP/NCAR reanalysis and (b) ERA-Interim.

level jet, we compared the relative roles of the jet intensities at five levels (1000, 925, 850, 700, and 600 hPa) in connection with the East Asian summer monsoon rainfall. Their relationships on the interannual timescale are discussed here. A Gaussian filter with a window width of 9 yr was used to isolate the interannual timescale. The results (figures omitted) show that positive correlations (strong jet with strong precipitation, and vice versa) extend from the middle reaches of the Yellow-Yangtze River basin. However, larger coherent regions of strong positive correlation over the Yellow-Yangtze River basin are more evident at the higher level than at the lower level.

When the WSMJ index, which includes variations of the higher-level jet, and the summer precipitation dataset from GPCC (Fig. 4a) and NCEP/NCAR (Fig. 4b) are correlated, similar patterns emerge and the positive correlation areas are largest. We defined a Yellow-Yangtze River basin precipitation index based on the correlations shown in Figs. 4a and 4b, averaging JJA rainfall data from GPCC over 29°–36°N, 107°–117°E. The jets at 925 and 700 hPa represent the lower- and higher-level jets, respectively. The statistical relationship between Yellow-Yangtze River basin rainfall and SMJ intensity is further verified in Figs. 4c–e, which shows the interannual variations of the jet index at 925 (Fig. 4c) and 700 hPa (Fig. 4d), the WSMJ index (Fig. 4e), and the Yellow-Yangtze basin precipitation indices. Compared with the jet index at 925 hPa, the relationship between the jet index at 700 hPa and precipitation indices are more highly correlated, with a correlation coefficient of 0.527 that exceeds the 99% confidence level. Interannual variations of the WSMJ index are also significantly correlated with Yellow-Yangtze River basin precipitation, with a correlation coefficient of 0.594, also exceeding the 99% confidence level. Traditionally, the jet at 925 hPa has been thought to be more important than the jet at other levels because it is the core of the SMJ. However, our comparison shows that the jet index at 925 hPa has a weaker connection with the examined rainfall than does the WSMJ index. This may be because the wind near the surface may be more subject to the noise, such as heat exchange, surface friction, large terrain (Tibetan Plateau), and so on, causing less water vapor to be brought into the East Asian monsoon region by the lower-level jet than by the higher-level jet.

Figure 4f shows the 9-yr sliding correlation between the precipitation index and the jet index at 925 and 700 hPa, as well as the WSMJ index. The sliding correlation is unstable and insignificant before the late 1990s, but becomes stable and significant thereafter, especially for the jet index at 700 hPa and the WSMJ index. This increased correlation after the late 1990s may be due to the strengthened higher-level jet. As we all know, there are four branches of the East Asian monsoon moisture transport channel: 1) the moisture airflow crossing the equator by SMJ; 2) the southeast monsoon moisture airflow from the southwest side of the western Pacific subtropical high; 3) the cross-equatorial moisture airflow through the South China Sea along 105°E; and 4) the moisture airflow brought by the midlatitude westerly disturbance. The four branches converge in the Yangtze and Huaihe River valley and then flow to Korean Peninsula and Japan (Tao and Cheng, 1985; Tao, 1987; Huang et al., 1998). Therefore, the strengthened higher-level jet can augment the contribution of SMJ to the moisture transport to East Asia, which results in a closer relationship between rainfall and the WSMJ.

To develop an understanding of the underlying atmospheric circulation anomalies associated with the connection between the WSMJ index and Yellow-Yangtze River basin precipitation during JJA, we examined the wind speed anomalies at 700 hPa over East Asia and the vertical circulation along 107°–117°E associated with the WSMJ index (Fig. 5). The climatological wind at 700 hPa in JJA (Fig. 5a) shows that the Yellow-Yangtze region is located at the junction of the westerlies and southwesterlies. As shown in Figs. 5b and 5c, because of the increased WSMJ intensity, the western Pacific subtropical high (WPSH) strengthens and shifts southward and westward, and the Yellow-Yangtze River basin is controlled by the consistent upward movement of the whole troposphere. Then, the strengthened WPSH causes the southwesterlies that originate from the SMJ to shift

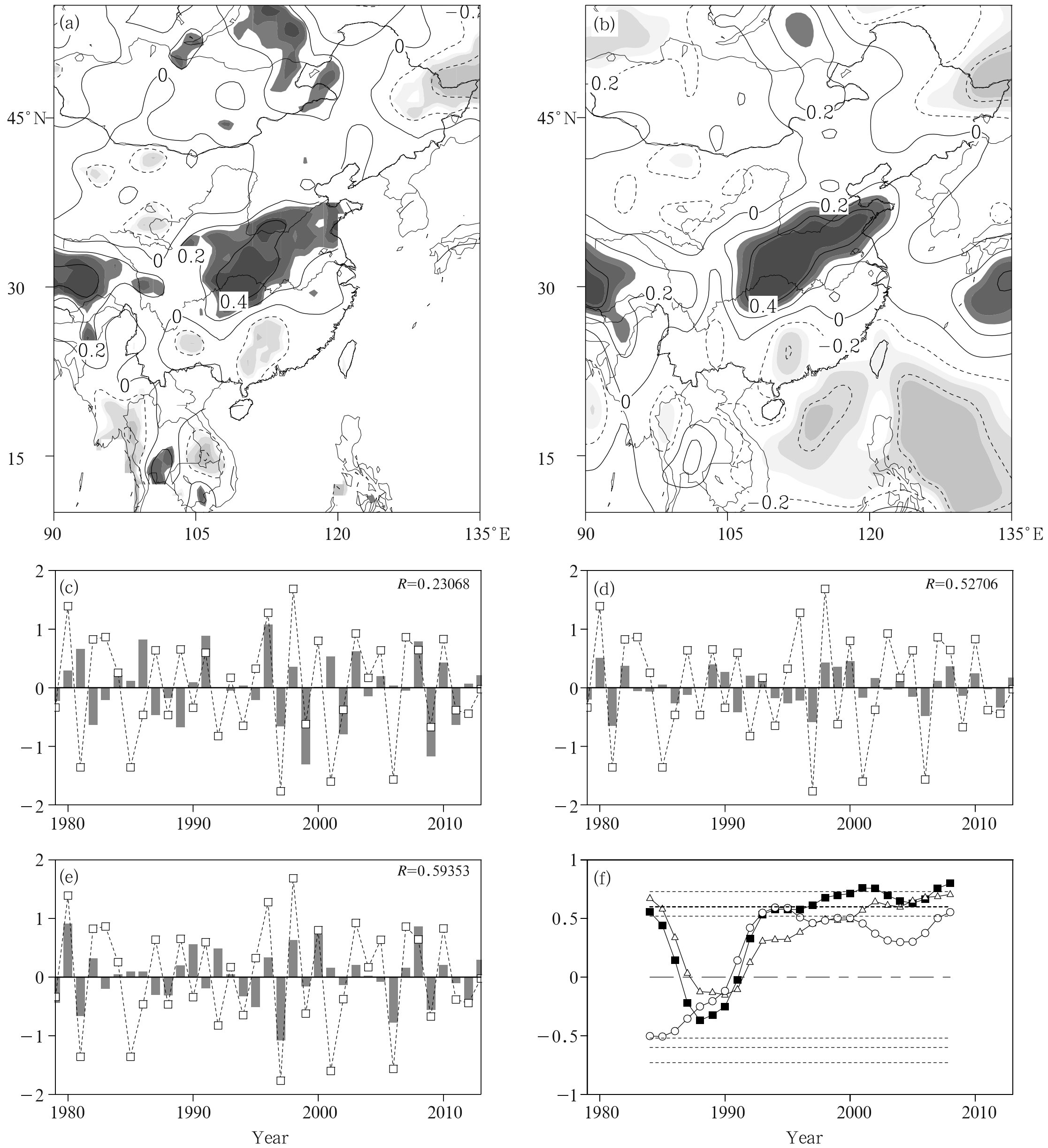

Fig. 4. Correlations between the WSMJ index and the summer precipitation from (a) GPCC data and (b) NCEP/NCAR reconstructed precipitation data during 1979–2013 for the 9-yr high-pass filtered data. Light to dark shadings indicate 90%, 95%, and 99% confidence levels. The time series of Yellow-Yangtze River basin precipitation index (dashed line with open squares in (c), (d), and (e)) from the GPCC data and the jet index at 925 (c; grey bar) and 700 hPa (d; grey bar), as well as the WSMJ index (e; grey bar), the correlation coefficients of their combinations are shown in the right top of (c), (d), and (e). (f) Moving correlation of Yellow-Yangtze River basin precipitation index with the jet index at 925 (solid line with dot) and 700 hPa (solid line with hollow triangle), as well as the WSMJ (solid line with square) indices, obtained by using a 9-yr window; the horizontal dashed lines show the 90%, 95%, and 99% significance levels.

northward and westward, causing strengthening of the southwesterly flow in the Yellow-Yangtze River basin. This means that more moisture is transported into the Yellow-Yangtze River basin and increased rainfall is expected to occur.

4. Causes of the interdecadal turning of SMJ vertical structure

4.1 Thermal contrast near the Somalia coast

Our discussion in Section 3.1 showed that there

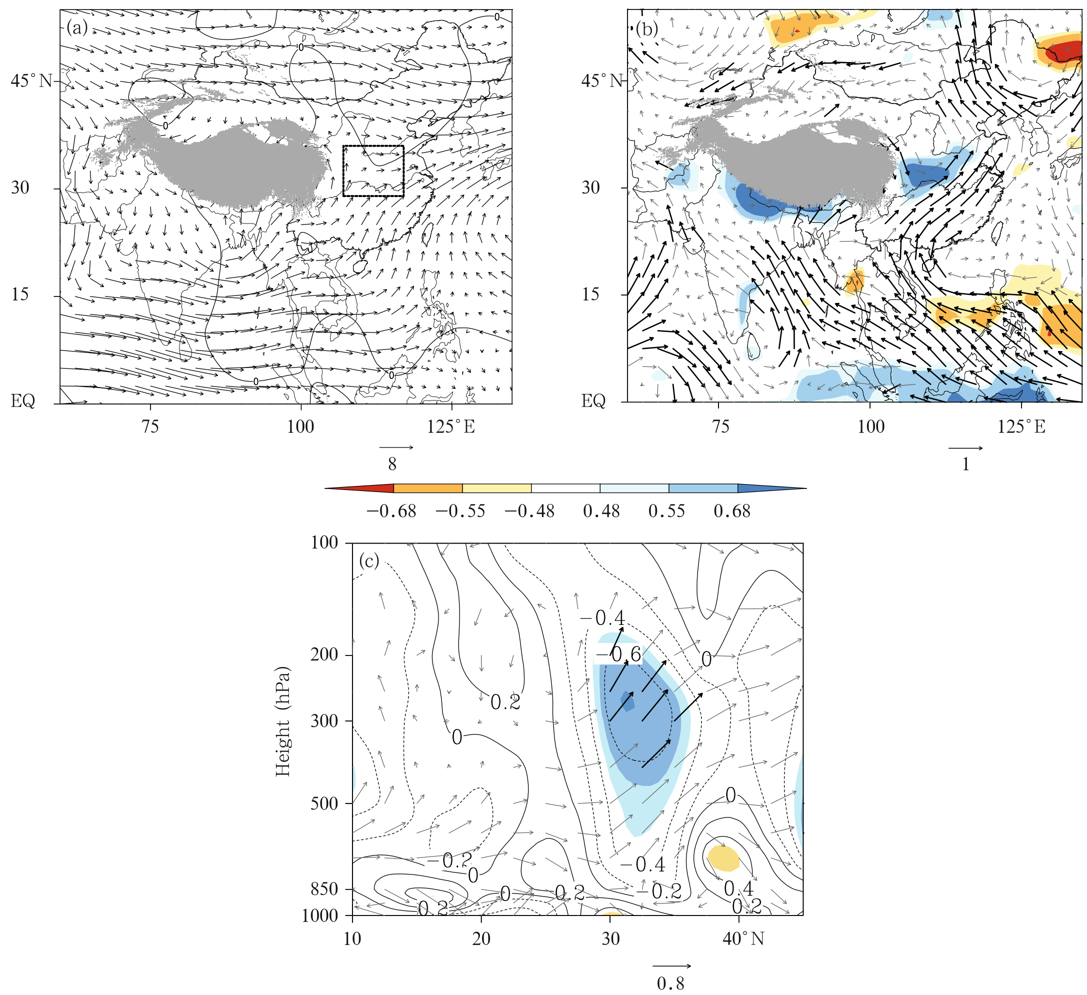

Fig. 5. (a) Climatological summer wind speed (m s^{-1}) at 700 hPa for 1979–2013. Simultaneous correlations of the WSMJ index with (b) the 700-hPa wind anomaly (vector) and precipitation anomaly (shaded), as well as (c) the vertical circulation (consisting of meridional wind and vertical p-velocity; vector) and vertical p-velocity (contour and shaded) along 107°–117°E for 1998–2010 in JJA. Light to dark shadings indicate 90%, 95%, and 99% confidence levels. The black bold arrows denote values significant at the 95% confidence level. All data were high-pass filtered by using a 9-yr window. The grey shadings in (a) and (b) indicate the domain of the Tibetan Plateau.

appears to be an interdecadal transition point in the vertical structure of the SMJ around the late 1990s, with the lower-level (higher-level) jet stronger (weaker) before the late 1990s and weaker (stronger) afterwards. However, what has caused the inverse change between the lower- and higher-level jets in the late 1990s?

To investigate the possible mechanism, we calculated the composite difference of air temperature and vertical circulation consisting of meridional wind and vertical velocity along 40°–55°E for the 1998–2010 mean minus the 1980–1992 mean during JJA (Fig. 6). Clearly, for the post-1995 period, in the tropics, there are meridional thermal contrast anomalies, with the warm anomaly centered around 10°S inclined northward with altitude (Fig. 6a). The north (south) of equator is relatively cold (warm) below 700 hPa, while exactly the reverse is the case above 700 hPa. As a result of these meridional thermal contrast anomalies, the heating differential and the pressure differential between north and south of the equator are formed (Murakami et al., 1970) such that descent anomalies north of the equator and ascent anomalies south of the equator, with two anomaly cells, occur (Fig. 6b). One is in the higher troposphere (at about 400 hPa) and the other is in the lower troposphere (at about 850 hPa). This implies that the northern summer Hadley cell, as stated by Oort and Rasmussen (1970), consisting of ascent near 10°N and descent near 25°S becomes weaker. Then, the lower tropospheric cell results in the higher-level southerly anomalies and lower-level northerly anomalies over the SMJ region. For the pre-1995 period, this situation is simply reversed.

The contribution of the meridional thermal contrast anomalies near the equator to the interdecadal transition of the inverse change between the lower- and higher-level jets is further confirmed in Fig. 7, which shows a cross-section of the altitude-time evolution of the meridional thermal contrast over the tropics, as well as the associated EOF analysis. The meridional thermal contrast is defined as the difference between the areal mean air temperature averaged over 0°–15°N, 40°–55°E and that averaged over 15°S–0°, 40°–55°E. During 1979–2013, the meridional thermal

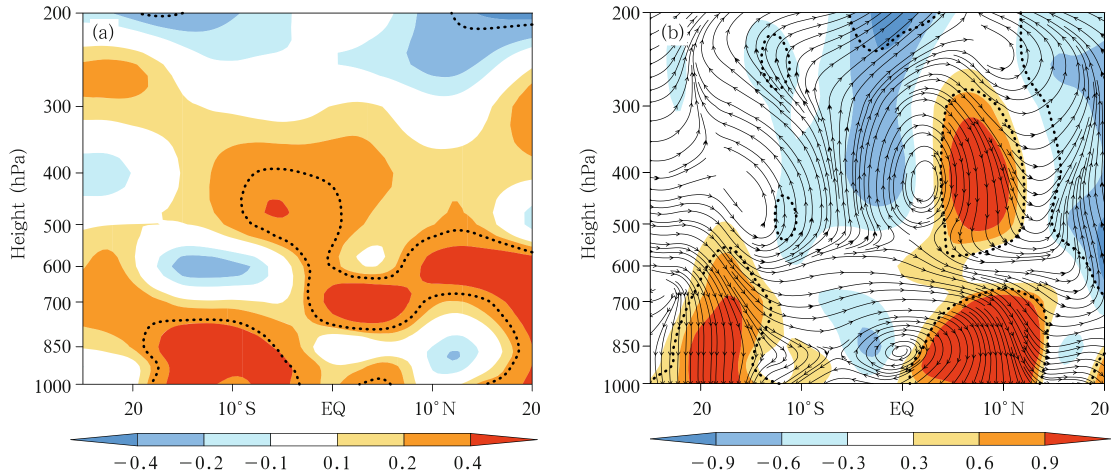

Fig. 6. Composite differences (1998–2010 mean minus 1980–1992 mean) for (a) air temperature at different levels (contour interval 0.2°C), and (b) vertical circulation (vector; consisting of meridional wind speed (m s^{-1}) and vertical p-velocity (Pa s^{-1})) and vertical p-velocity (Pa s^{-1}; shaded) along 40°–55°E near the SMJ region in JJA. The vertical p-velocity has been multiplied by –100. Areas encircled by black bold dashed lines denote differences significant at the 95% confidence level.

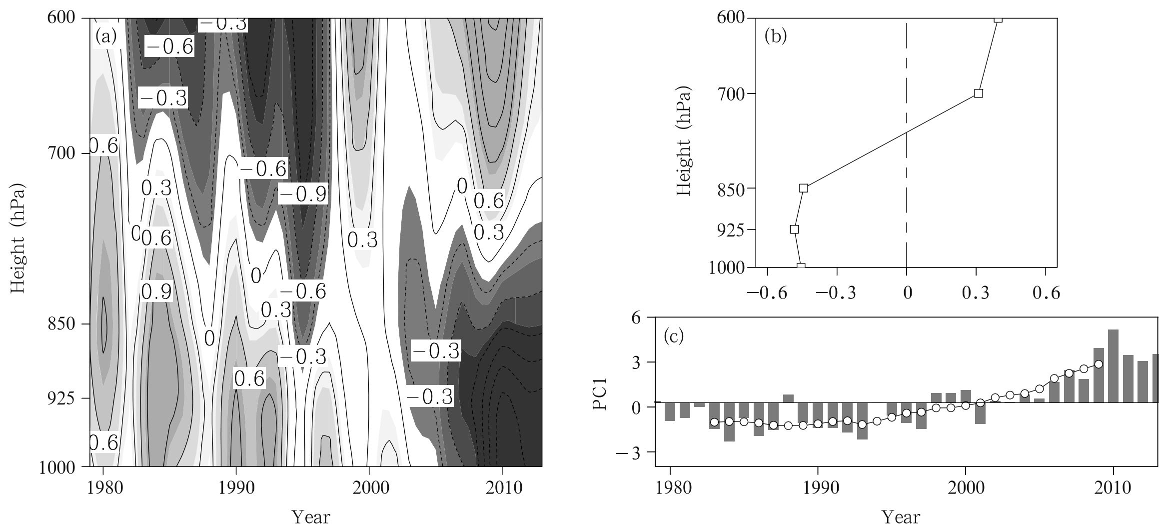

Fig. 7. (a) Cross-section of altitude-time evolution of the meridional thermal contrast (defined as the air temperature difference averaged over 0°–15°N, 40°–55°E minus that averaged over 0°–15°S, 40°–55°E in JJA), (b) the first EOF decomposition of (a), and (c) PC1 of the EOF decomposition (bar) and its 9-yr running mean (curve).

contrast near the SMJ region during the boreal summer decreased at lower levels but increased markedly at higher levels, which is very similar to the variation characteristic in the vertical structure of the SMJ. Its interdecadal transition point was also around 1995.

4.2 Roles of the southern Indian Ocean SST

The above analysis reveals that the meridional thermal contrast anomalies near the equator may be responsible for the interdecadal transition of the inverse change between the lower- and higher-level jets in the late 1990s; but what causes the the meridional thermal contrast anomalies near the equator? With a large heat capacity and thermal inertia, the oceans' influence on the atmospheric circulation is persistent, in the sense that the SST anomalies at the previous seasons can affect the atmospheric circulation at the subsequent seasons. Therefore, it is necessary to consider the role of the ocean in spring. To develop a better understanding of the dominant modes of variability, anomalies were decomposed by using the empirical orthogonal function (EOF) technique for the southern Indian Ocean basin between 55°S and the equator. These SST anomalies (SSTAs) are departures from a monthly mean climatology for the period 1979–2013. The second EOF mode, which explains about 14.7% of the total variance, shows a three-pole pattern oriented in the northeast-southwest direction (Fig. 8a). In addition, the time coefficient has strengthened since 1995 (Fig. 8b), which indicates that the three-pole pattern in the southern Indian Ocean also experienced an interdecadal change around the late 1990s.

Figures 9a and 9b show the regression map of the southern Indian Ocean SST in spring and summer, respectively, against the first principle component (PC1) of the meridional thermal contrast near the SMJ region. To allow us to consider the influence of the SST warming trend, the linear trend was removed from the SST data. During the two seasons, the SSTA distributions are similar to the well-defined three-pole SSTAs in the southern Indian Ocean. The resemblance between the three-pole pattern of the regression plots

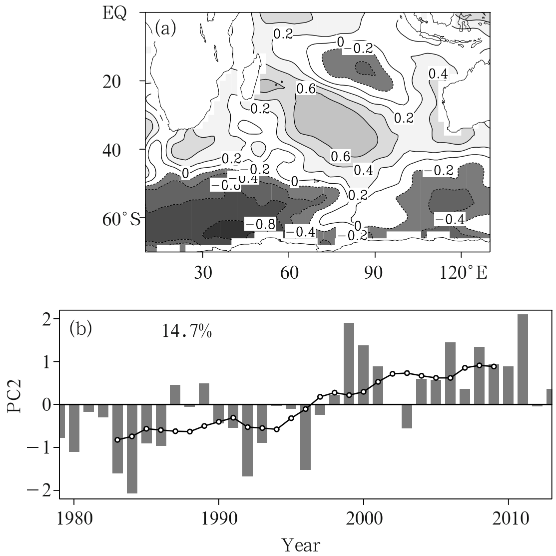

Fig. 8. (a) Spatial pattern of EOF2 of the Indian Ocean SSTA for MAM (March, April, May) and (b) PC2 of the EOF decomposition.

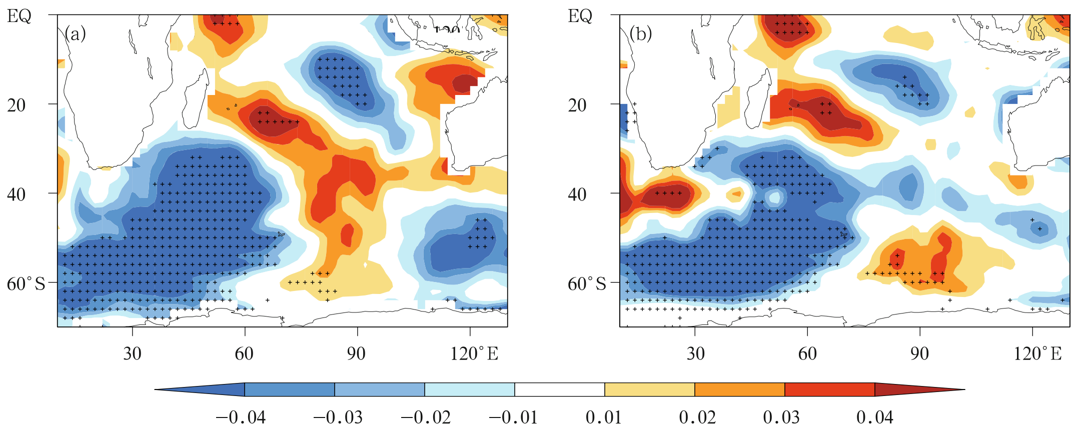

Fig. 9. Regression of the Indian Ocean SSTA in (a) spring and (b) summer against PC1 of the meridional thermal contrast near the SMJ region for the detrended SST data. Areas covered by black plus signs denote values significant at 95% confidence level.

and the second EOF mode of the southern Indian Ocean SSTA in Fig. 8 suggests that the meridional thermal contrast anomalies near the equator are possibly caused by the three-pole pattern of the southern Indian Ocean, which can persist from spring to the following summer.

The importance of the three-pole pattern is supported by the regressions of the air temperature and wind anomalies in JJA at 925 and 700 hPa against the PC2 of the three-pole pattern in the southern Indian Ocean (Fig. 10). As shown in Figs. 10a and 10b, the relatively warm (cold) anomaly south (north) of the equator leads to cross-equatorial northerly anomalies at 925 hPa, while the relatively warm (cold) anomaly north (south) of the equator leads to cross-equatorial southerly anomalies at 700 hPa. The wind anomalies at 700 hPa are much stronger than those at 925 hPa, which may have led to the stronger high-level cross-equatorial southerlies over the SMJ regions after 1995.

5. Conclusions

This study has demonstrated that the correlationship of higher-level SMJ intensity (which has a larger year-to-year amplitude than the lower-level jet) with the East Asian summer monsoon is higher than that of the lower-level jet. Consequently, we defined a new jet index, the WSMJ index, based on the average meridional wind at all levels. The WSMJ is closely related to the East Asian summer monsoon rainfall on interannual timescales, especially after the late 1990s, with positive correlations over the Yellow-Yangtze River basin. The increased WSMJ intensity strengthens and shifts the WPSH southward and westward, causing the Yellow-Yangtze River basin to be controlled by the consistent upward movement and the southwesterly anomalies through the whole troposphere. More moisture is transported to the Yellow-Yangtze River basin and more precipitation occurs.

Variations in the vertical structure of the SMJ show that the higher- and lower-level jet changes are out of phase with an interdecadal transition occurring around the late 1990s. Probable causes of the inverse change between the lower- and higher-level jets in the late 1990s were analyzed in detail. During the by the meridional thermal contrast anomalies near the equa-

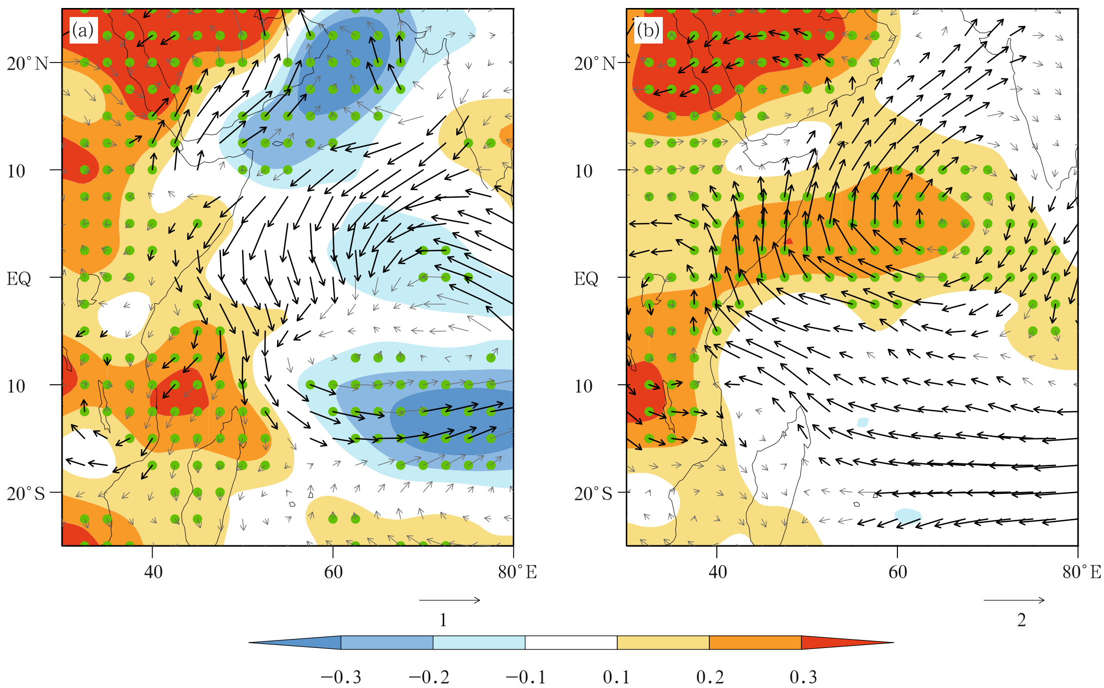

Fig. 10. Regressions of the air temperature (shaded) and wind (vector) anomalies in JJA at (a) 925 and (b) 700 hPa against PC2 of the Indian Ocean SSTA for MAM. Area coverd by green dots and black bold arrows denote values significant at the 95% confidence level.

tor, with the warm anomaly centered around 10°S and inclined northward with altitude. Consequently, relatively cold (warm) anomalies north of the equator and warm (cold) anomalies south of the equator at 925 (700) hPa caused lower-level (higher-level) cross-equatorial northerly (southerly) anomalies. The second EOF mode of the southern Indian Ocean SSTA in spring shows a three-pole pattern and the time coefficient of it also experienced an interdecadal change in the late 1990s. Thus, the meridional thermal contrast anomalies near the coast of Somalia may be attributed to this three-pole pattern, which can persist from spring to the following summer. The regression map of the southern Indian Ocean SST in spring and summer against the PC1 of the meridional thermal contrast also supports this conclusion. Our studies way help to improve the understanding of the SMJ's establishment and formation, as well as its impact on the Asian summer monsoon.

REFERENCES

Annamalai, H., J. M. Slingo, K. R. Sperber, et al., 1999: The mean evolution and variability of the Asian summer monsoon: Comparison of ECMWF and NCEP-NCAR reanalyses. *Mon. Wea. Rev.*, **127**, 1157–1186.

Bannon, P. R., 1979a: On the dynamics of the East African jet. I: Simulation of mean conditions for July. *J. Atmos. Sci.*, **36**, 2139–2152.

Bannon, P. R., 1979b: On the dynamics of the East African jet. II: Jet transients. *J. Atmos. Sci.*, **36**, 2153–2168.

Bannon, P. R., 1982: On the dynamics of the East African jet. III: Arabian sea branch. *J. Atmos. Sci.*, **39**, 2267–2278.

Boos, W. R., and K. A. Emanuel, 2009: Annual intensification of the Somali jet in a quasi-equilibrium framework: Observational composites. *Quart. J. Roy. Meteor. Soc.*, **135**, 319–335.

Bunker, A. F., 1965: *Interaction of the Summer Monsoon Air with the Arabian Sea: Preliminary Analysis.* Commercial Printing Press, 3–16.

Cadet, D., and M. Desbois, 1981: A case study of a fluctuation of the Somali jet during the Indian summer monsoon. *Mon. Wea. Rev.*, **109**, 182–187.

Chakraborty, A., R. S. Nanjundiah, and J. Srinivasan, 2009: Impact of African orography and the Indian summer monsoon on the low-level Somali jet. *Int. J. Climatol.*, **29**, 983–992.

Chen, M., P. Xie, J. E. Janowiak, et al., 2002: Global land precipitation: A 50-yr monthly analysis based on gauge observations. *J. Hydrometeor.*, **3**, 249–266.

Chen Bing, Guo Pinwen, and Xiang Yuchuan, 2005: Relationship between summer cross-equatorial flows and ENSO. *J. Nanjing Inst. Meteor.*, **28**, 36–43. (in Chinese)

Cong Jing, Guan Zhaoyong, and Wang Lijuan, 2007: Interannual (interdecadal) variabilities of two cross-equatorial flows in association with the Asian summer monsoon variations. *J. Nanjing Inst. Meteor.*, **30**, 779–785. (in Chinese)

Dai Wei and Xiao Ziniu, 2014: Multi-time scale variation characteristics of Somali jet and its contact with precipitation in China. *J. Trop. Meteor.*, **30**, 368–376. (in Chinese)

Ding Yihui, 2005: *Advanced Synoptic Meteorology.* China Meteorological Press, Beijing, 585 pp. (in Chinese)

Findlater, J., 1969a: A major low-level air current near the Indian Ocean during the northern summer. *Quart. J. Roy. Meteor. Soc.*, **95**, 362–380.

Findlater, J., 1969b: Inter-hemispheric transport of air in the lower troposphere over the western Indian Ocean. *Quart. J. Roy. Meteor. Soc.*, **95**, 400–403.

Findlater, J., 1977: Observational aspects of the low level cross equatorial jet stream of the western Indian Ocean. *Pure Appl. Geophys.*, **115**, 1251–1262.

Gao Hui and Xue Feng, 2006: Seasonal variation of the cross-equatorial flows and their influences on the onset of South China Sea summer monsoon. *Climatic Environ. Res.*, **11**, 57–68. (in Chinese)

Halpern, D., and P. M. Woiceshyn, 2001: Somali jet in the Arabian Sea, El Niño, and Indian rainfall. *J. Climate*, **14**, 434–441.

Hart, J. E., 1977: On the theory of the East African low level jet stream. *Pure Appl. Geophys.*, **115**, 1263–1282.

Honda, M., J. Inous, and S. Yamane, 2009: Influence of low Arctic sea-ice minima on anomalously cold Eurasian winters. *Geophys. Res. Lett.*, **36**, L08707, doi: 10.1029/2008GL037079.

Huang Ronghui, Zhang Zhenzhou, Huang Gang, et al., 1998: Characteristics of the water vapor transport in East Asian monsoon region and its difference from that in South Asian monsoon region in summer. *Chinese J. Atmos. Sci.*, **22**, 460–469. (in Chinese)

Joseph, P. V., and P. L. Raman, 1966: Existence of low-level westerly jet stream over Peninsular India during July. *Indian J. Meteor. Geophys.*, **17**, 407–410.

Kalnay, E., M. Kanamitsu, R. Kistler, et al., 1996: The NCEP/NCAR 40-yr reanalysis project. *Bull. Amer. Meteor. Soc.*, **77**, 437–471.

Krishnamurti, T. N., J. Molinari, and H. L. Pan, 1976: Numerical simulation of the Somali jet. *J. Atmos. Sci.*, **33**, 2350–2362.

Krishnamurti, T. N., and V. Wong, 1979: Planetary boundary-layer model for the Somali jet. *J. Atmos. Sci.*, **36**, 1895–1907.

Lei Xiaochun and Yang Xiuqun, 2008: Interannual variation characteristic of Eastern Hemispheric cross-equatorial flow and its contemporaneous relationships with temperature and rainfall in China. *J. Trop. Meteor.*, **24**, 127–135. (in Chinese)

Lin Meijing, Fan Ke, and Wang Huijun, 2008: Somali jet changes under the global warming. *Acta Meteor. Sinica*, **22**, 502–510. (in Chinese)

Li Puzhong and Lou Guanghu, 1987: A study on the passages of cross-equatorial current during the southern monsoon. *Chinese J. Atmos. Sci.*, **11**, 313–319. (in Chinese)

Li Xiaofeng, Guo Pinwen, Dong Lina, et al., 2006: Onset process of summer Somali jet and the possible influenced mechanism. *Trans. Atmos. Sci.*, **29**, 599–605. (in Chinese)

Murakami, T., R. Godbole, and R. R. Kelkar, 1970: Numerical simulation of the monsoon along 80°E. Pro. Conf. Summer Monsoon of Southeast Asia, Navy Wea. Res. Fac., Norfolk, Va., 39–51.

Oort, A. H., and E. M. Rasmusson, 1970: On the annual variation of the monthly mean meridional circulation. *Mon. Wea. Rev.*, **98**, 423–442.

Pu, B., and K. H. Cook, 2010: Dynamics of the West African westerly jet. *J. Climate*, **23**, 6263–6276.

Pu, B., 2012: Role of the West African westerly jet in Sahel rainfall variations. *J. Climate*, **25**, 2880–2896.

Qian Yongfu, Wang Qianqian, Dong Yiping, et al., 1987: Numerical experiment of Somali jet. *Chinese J. Atmos. Sci.*, **11**, 176–184. (in Chinese)

Qiu Jinjing and Sun Zhaobo, 2013: Variation characteristics of the vertical structure of the summer Somali cross-equatorial flow and its relationship with East Asian summer monsoon activity. *Chinese J. Atmos. Sci.*, **37**, 1129–1142. (in Chinese)

Qiu Jinjing, Sun Zhaobo, and Deng Weitao, 2014: The interdecadal variations of the vertical structure of the summer Somali cross-equatorial flow. *Acta Meteor. Sinica*, **72**, 318–336, doi: 10.11676/qxxb2014.005. (in Chinese)

Rodwell, M. J., and B. J. Hoskins, 1995: A model of the Asian summer monsoon. Part II: Cross-equatorial flow and PV behavior. *J. Atmos. Sci.*, **52**, 1341–1356.

Rudolf, B., H. Hauschild, W. Ruth, et al., 1994: Terrestrial precipitation analysis: Operational method and required density of point measurements. *Global Precipitation and Climate Change*, Dubois, M., and M. Desalmand, Eds., 173–186.

Shi Neng, Feng Guolin, Gu Junqiang, et al., 2007: The climatological variation of global cross-equatorial flow for the period of 1948–2004. *J. Trop. Meteor.*, **23**, 326–332. (in Chinese)

Shi Ning, Shi Danping, and Yan Mingliang, 2001: The effects of cross-equatorial current on South China Sea monsoon onset and drought/flood in East China. *J. Trop. Meteor.*, **17**, 405–415. (in Chinese)

Shi Wenjing and Xiao Ziniu, 2013: Variation of the cross-equatorial moisture transport in Somali and its impact on China early summer rainfall in nearly 60 years. *Meteor. Mon.*, **39**, 39–45. (in Chinese)

Smith, T. M., and R. W. Reynolds, 2004: Improved extended reconstruction of SST (1854–1997). *J. Climate*, **17**, 2466–2477.

Simmons, A., S. Uppala, D. Dee, et al., 2007: ERA-Interim: New ECMWF reanalysis products from 1989 onwards. *ECMWF Newsletter*, **110**, 25–35.

Sterl, A., 2004: On the (in)homogeneity of reanalysis products. *J. Climate*, **17**, 3866–3873.

Tang Bi, Guo Pinwen, and Yang Liping, 2009: Interannual variation of summer cross-equatorial flow in lower troposphere of Eastern Hemisphere. *Trans. Atmos. Sci.*, **32**, 98–305. (in Chinese)

Tao, S. Y., and L. X. Chen, 1985: The East Asian summer monsoon. Proceedings of the International Conference on Monsoon in the Far East. Tokyo, Nov. 5–8, 1–11.

Tao, S., 1987: A review of recent research on the East Asian summer monsoon in China. *Monsoon Meteorology*, Chang, C. P., and T. N. Krishnamurti, Eds., Oxford University Press, 60–92.

Wang Huijun and Xue Feng, 2003: Interannual variability of Somali jet and its influences on the inter-hemispheric water vapor transport and on the East

Asian summer rainfall. *Chinese J. Geophys.*, **46**, 18–25. (in Chinese)

Wang Weiping and Yang Xiuqun, 2008: Variation of Somali jet and its impact on East Asian summer monsoon and associated China rainfall anomalies. *J. Meteor. Sci.*, **28**, 139–146. (in Chinese)

Wu, B., J. Overland, and R. D'Arrigo, 2012: Anomalous Arctic surface wind patterns and their impacts on September sea ice minima and trend. *Tellus A*, **64**, 18590.

Wu, B. Y., R. H. Zhang, R. D'Arrigo, et al., 2013: On the relationship between winter sea ice and summer atmospheric circulation over Eurasia. *J. Climate*, **26**, 5523–5536, doi: 10.1175/JCLI-D-12-00524.1.

Xie Lei, Sun Zhaobo, Li Zhongxian, et al., 2013: Vertical structure of summer Somali cross-equatorial flow and its relationship with South Asian monsoon. *J. Meteor. Sci.*, **33**, 37–42. (in Chinese)

Xu Zhongfeng, Qian Yongfu, and Fu Congbin, 2010: The role of land–sea distribution and orography in the Asian monsoon. Part II: Orography. *Adv. Atmos. Sci.*, **27**, 528–542.

Zhu Yali, 2012: Variations of the summer Somali and Australian cross-equatorial flows and the implications for the Asian summer monsoon. *Adv. Atmos. Sci.*, **29**, 509–518.